The Astrophysical Journal, 722:1854–1863, 2010 October 20 doi:10.1088/0004-637X/722/2/1854

THE FREQUENCY OF LOW-MASS EXOPLANETS. II. THE "PERIOD VALLEY"

Robert A. Wittenmyer[1], Simon J. O'Toole[2], H. R. A. Jones[3], C. G. Tinney[1], R. P. Butler[4], B. D. Carter[5], and J. Bailey[1]
[1] Department of Astrophysics, School of Physics, University of NSW, 2052, Australia; rob@phys.unsw.edu.au
[2] Anglo-Australian Observatory, P.O. Box 296, Epping, 1710, Australia
[3] Centre for Astrophysics Research, University of Hertfordshire, College Lane, Hatfield, Herts AL10 9AB, UK
[4] Department of Terrestrial Magnetism, Carnegie Institution of Washington, 5241 Broad Branch Road NW, Washington, DC 20015-1305, USA
[5] Faculty of Sciences, University of Southern Queensland, Toowoomba, Queensland 4350, Australia
Received 2010 March 23; accepted 2010 August 25; published 2010 October 5

ABSTRACT

Radial-velocity planet search campaigns are now beginning to detect low-mass "Super-Earth" planets, with minimum masses $M \sin i \lesssim 10\,M_{\oplus}$. Using two independently developed methods, we have derived detection limits from nearly four years of the highest-precision data on 24 bright, stable stars from the Anglo-Australian Planet Search. Both methods are more conservative than a human analyzing an individual observed data set, as is demonstrated by the fact that both techniques would detect the radial-velocity signals announced as exoplanets for the 61 Vir system in 50% of trials. There are modest differences between the methods which can be recognized as arising from particular criteria that they adopt. What both processes deliver is a *quantitative* selection process such that one can use them to draw quantitative conclusions about planetary frequency and orbital parameter distribution from a given data set. Averaging over all 24 stars, in the period range $P < 300$ days and the eccentricity range $0.0 < e < 0.6$, we could detect 99% of planets with velocity amplitudes $K \gtrsim 7.1$ m s^{-1}. For the best stars in the sample, we are able to detect or exclude planets with $K \gtrsim 3$ m s^{-1}, corresponding to minimum masses of 8 $M_{\oplus}$ ($P =$ 5 days) or 17 $M_{\oplus}$ ($P = 50$ days). Our results indicate that the observed "period valley," a lack of giant planets ($M > 100\,M_{\oplus}$) with periods between 10 and 100 days, is indeed real. However, for planets in the mass range 10–100 $M_{\oplus}$, our results suggest that the deficit of such planets may be a result of selection effects.

Key words: planetary systems – techniques: radial velocities

1. INTRODUCTION

Extrasolar planet detections are inexorably pushing toward ever-lower masses, and it seems that each new mass threshold spawns an unavoidably anthropocentric moniker. First, in 1995, were the "hot Jupiters" (or "roasters"; Sudarsky et al. 2000), with minimum masses $m \sin i$ greater than the mass of Jupiter (Mayor & Queloz 1995). The earliest planet discoveries fell into this category due to the well-known radial-velocity selection bias toward detecting massive planets in short-period orbits ($P \lesssim$ 10 days). The discovery of several Neptune-mass ($= 17.4\,M_{\oplus}$) planets in 2004 (McArthur et al. 2004; Santos et al. 2004; Bonfils et al. 2005) brought the "hot Neptune" into common parlance. Most recently, the discovery of planets with $m \sin i$ less than 10 Earth masses has prompted the somewhat misleading appellation of "Super-Earth." These planets, of course, are not likely to bear any resemblance to Earth, and models of the composition of such objects strongly suggest that almost all of these worlds possess thick atmospheres surrounding a core of rock and ice (Seager et al. 2007; Adams et al. 2008).

The Anglo-Australian Planet Search (AAPS) has been in operation at the 3.9 m Anglo-Australian Telescope (AAT) for 11 years and has published 36 exoplanet discoveries. By integrating for at least 20 minutes on each target in order to average over the stellar p-mode oscillations (O'Toole et al. 2008), the AAPS now achieves velocity precision approaching 1 m s^{-1} for bright, inactive stars (O'Toole et al. 2009c). Since 2005 June, the AAPS has been routinely implementing this observing strategy, which has (together with long continuous observing blocks) proven instrumental in our recent discovery of a Super-Earth and two Neptune-mass planets orbiting 61 Vir (Vogt et al. 2010).

In O'Toole et al. (2009c), we explored the frequency of planets with periods less than ∼20 days. In that work, we derived detection sensitivities from a continuous 48-night observing campaign targeting 24 bright, stable stars. The stars have spectral types between G0 and K5, and they range in mass from 0.77 to 1.28 $M_{\odot}$; complete details are given in Table 1 of O'Toole et al. (2009c). In this paper, we consider periods ranging up to 300 days, now making use of nearly four years of high-quality data on these 24 stars from the AAPS. The observational data are summarized in Table 1, and the parameters of the five planets which have been found in this sample are given in Table 2. We also bring two independent simulation algorithms to bear on these data to derive extremely tight limits on planetary companions in the range 2 days $< P <$ 300 days. The planetary periods and masses probed by these data are interesting for two reasons. First, this region includes the "period valley" noted by Jones et al. (2003) and Udry et al. (2003)—a lack of planets with orbital periods of 10–100 days. Second, the large amount of high-precision data used here enables the detection of potentially terrestrial-mass planets. Core-accretion simulations which include Type I migration (Ida & Lin 2004, 2008b) predict an abundance of planets with masses less than about 10 $M_{\oplus}$ orbiting within 1 AU and a lack of planets with higher masses in that region (the "planet desert"). The large, extremely high precision data set analyzed here represents one of the first able to test these predictions.

In Section 2, we describe the two methods used to derive detection limits from these data. Section 3 presents the results and discusses differences between the two methods. In Section 4, we further discuss the implications of our results with regards to the underlying distribution of exoplanets.

2. COMPUTATIONAL METHODS

There are two ways to approach the input data for a detection-limit computation: using the actual radial-velocity data

Table 1
Summary of Radial-velocity Data

Star	N	rms ($m\ s^{-1}$)	$\langle\sigma\rangle$ ($m\ s^{-1}$)
HD 1581	58	2.81	0.95
HD 4308	77	2.92[a]	1.09
HD 10360	31	3.77[b]	0.90
HD 10361	31	3.20[b]	0.84
HD 10700	95	2.65	0.86
HD 16417	55	2.66[a]	0.86
HD 20794	78	3.43	0.81
HD 23249	64	3.16	0.56
HD 26965	55	4.80	0.76
HD 28255A	37	7.57	1.18
HD 43834	78	4.27	0.80
HD 53705	80	3.09	1.21
HD 72673	50	2.66	1.06
HD 73524	44	4.22	1.28
HD 84117	83	5.00	1.33
HD 100623	62	4.08	1.00
HD 102365	97	2.49	0.89
HD 114613	106	4.25	0.78
HD 115617	94	4.29	0.74
HD 122862	49	3.81	1.27
HD 128620	33	1.94[c]	0.40
HD 128621	42	2.76[c]	0.56
HD 136352	78	4.34	1.07
HD 146233	48	3.91	1.02

Notes.
[a] After removal of known planet's orbit.
[b] Residuals of linear fit.
[c] Residuals of quadratic fit.

(Wittenmyer et al. 2006; Endl et al. 2002) or creating simulated data sets using the observation dates and uncertainties of the real data (O'Toole et al. 2009a; Cumming et al. 1999). We have employed independent methods using each of these approaches to determine the types of planets to which these data were sensitive.

2.1. Simulated Data

The first simulation technique, described fully in O'Toole et al. (2009a), seeks to recover simulated Keplerian signals (with appropriate noise terms arising from measurement uncertainties and stellar jitter) sampled at the epochs of the actual data and retaining the original uncertainties of the actual data. The simulated velocity curves are analyzed using the two-dimensional Lomb–Scargle periodogram (O'Toole et al. 2007, 2009a) which extends the standard Lomb–Scargle periodogram to search eccentricity as well as period space.

The simulated observations for this study were constructed in the following way. We used a grid of periods, eccentricities, and planet masses as input in the same way as O'Toole et al. (2009a), with periods in the range 2–320 days, eccentricities from 0.0 to 0.6 in steps of 0.1, and masses of 0.005, 0.01, 0.02, 0.05, 0.1, 0.2, 0.5, and 1.0 M_J. Each set of parameters was simulated 100 times, leading to 72,800 simulated velocity curves for each of the 24 stars.

This approach does not use the standard F-test to determine the reliability of a detection. Instead, it uses four detection criteria as follows (O'Toole et al. 2009a). First, the rms of the simulated observations must be greater than or equal to the rms of the residuals of the best-fitting model to those data. That is, the scatter should decrease after the subtraction of a Keplerian model. Second, the measured semi-amplitude must be greater than or equal to twice the measured semi-amplitude uncertainty plus the rms of the residuals of the best-fitting model. Third, the measured period must be greater than or equal to twice the measured period uncertainty. Finally, the value of χ^2_ν must be less than or equal to 3. The last criterion is only useful when stellar jitter is not included, as discussed by O'Toole et al. (2009a); in this paper and O'Toole et al. (2009c)—where jitter is included—it is somewhat redundant. The other three criteria are a gauge of the reliability of a fit.

With these criteria, the method does not rely on the assumptions of the F-test. Its chief strengths lie in its ability to recover significantly eccentric orbits (O'Toole et al. 2009a) which would be undetectable using a standard Lomb–Scargle periodogram. In addition, because this method performs a full Keplerian fit to the simulated data, the distribution of orbital parameters derived from the fits provides valuable information on the biases inherent in fitting radial-velocity data (O'Toole et al. 2009a). For the rest of this paper, we will refer to this algorithm as Method 1.

2.2. Real Data

The second technique, described fully in Wittenmyer et al. (2006), adds the Keplerian signal of a simulated planet to the original data and then attempts to recover that signal using a Lomb–Scargle periodogram (Lomb 1976; Scargle 1982). Previous work using similar methodology includes Walker et al. (1995) and Endl et al. (2002). We will refer to this algorithm as Method 2. In this work, we required that the recovered period be within 5% of the injected period, and that its false-alarm probability (FAP) be less than 0.1%. As the null hypothesis of this method is that the data are purely noise and contain no signals due to real planets, the known planets HD 4308b (Udry et al. 2006) and HD 16417b (O'Toole et al. 2009b) must be treated differently. As noted in Wittenmyer et al. (2009), the velocity signature of an unknown planet can be altered by the presence of an additional (known) planet. Hence, we have determined the detection limits for HD 4308 and HD 16417 using the method of Wittenmyer et al. (2009) wherein the simulated planet is added prior to fitting for and removing the known planet's signal. For the Alpha Centauri system (HD 128620/1), we removed a quadratic fit to the data, which

Table 2
Planets from This Sample

Planet	Period (days)	T_0 (JD-2400000)	e	ω (deg)	K ($m\ s^{-1}$)	$M \sin i$ ($M_\oplus$)	a (AU)	Reference
HD 16417 b	17.24 ± 0.01	50099.7 ± 3.3	0.20 ± 0.09	77 ± 26	5.0 ± 0.4	22.1 ± 2.0	0.14 ± 0.01	O'Toole et al. (2009b)
HD 4308 b	15.609 ± 0.007	50108.5 ± 1.9	0.27 ± 0.12	210 ± 21	3.6 ± 0.3	13.0 ± 1.4	0.118 ± 0.009	O'Toole et al. (2009c)
HD 115617 b	4.2150 ± 0.0006	53369.166 ± (fixed)	0.12 ± 0.11	105 ± 54	2.12 ± 0.23	5.1 ± 0.5	0.050201 ± 0.000005	Vogt et al. (2010)
HD 115617 c	38.021 ± 0.034	53369.166 ± (fixed)	0.14 ± 0.06	341 ± 38	3.62 ± 0.23	18.2 ± 1.1	0.2175 ± 0.0001	Vogt et al. (2010)
HD 115617 d	123.01 ± 0.55	53369.166 ± (fixed)	0.35 ± 0.09	314 ± 20	3.25 ± 0.39	22.9 ± 2.6	0.476 ± 0.001	Vogt et al. (2010)

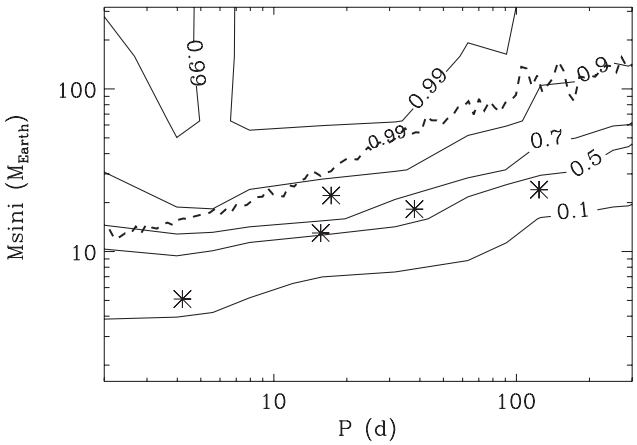

Figure 1. Detectabilities obtained from Method 1 (solid contours) averaged over all 24 stars, for planets with eccentricities from 0.0 to 0.6. Contours indicate the fraction of injected planets that were recovered. Results from Method 2 (99% recovery) for the same range of eccentricities are shown as a dotted line. The five announced planets in this sample are plotted as large asterisks.

provided a satisfactory approximation of the binary orbit over the short time period considered here. We also removed linear trends from the long-period binaries HD 10360 and HD 10361. Each star received seven trials at the 99% recovery level for trial signals with $e = 0.0$, 0.1, 0.2, 0.3, 0.4, 0.5, and 0.6. In addition, simulations at 90%, 70%, 50%, and 10% recovery were performed at $e = 0.0$ for each star.

This method is computationally faster than Method 1, since each trial only requires the computation of a simple periodogram, and there are considerably fewer such trials. Method 2 also has the advantage that the noise characteristics of the real data are preserved, whereas for simulated data, additional assumptions must be made about the noise term. However, it breaks down when there are fewer than ∼30 data points, as the reliability of the FAP calculation is strongly dependent on the number of data points. With limited data, even a very strong periodogram peak may fail to reach the 0.1% FAP level. This is less relevant for the current work, as all 24 stars considered here have at least 31 observations (Table 1). We note that Cumming et al. (2008) in their appendix give formulae for the FAP calculation in the regime of small *N*. For future work, the FAP calculations in Method 1 can be modified in this manner to better handle small *N*.

3. RESULTS

3.1. Detectabilities

For the purpose of this study, we define "detectability" as the fraction of simulated planets which were successfully recovered by the detection criteria employed by each method. To obtain a "big-picture" view of the types of planets detectable with our current data set, we have averaged the results over all stars and all eccentricities. Figure 1 shows the detectabilities from Method 1; the contours indicate the fraction of simulated planets that were recovered. The 99% detection limits obtained in this manner from Method 2 are overplotted as a dashed line. Results for each individual star are shown in Figures 2–13. The detectabilities obtained in this work are highly dependent on the characteristics of the data set; HD 20794 (Figure 5) has a large number of observations with little scatter ($N = 78$, rms = 3.43 m s^{-1}), whereas HD 28255a (Figure 6) has few data points and considerable scatter ($N = 37$, rms = 7.5 m s^{-1}). These results highlight the need to perform detection-limit computations on a star-by-star basis (O'Toole et al. 2009a) rather than "whole of sample." Table 3 summarizes the results from both methods for each star. We list the mean velocity amplitude *K* (averaged over all periods 2–300 days) which was recovered at the 99% and 50% levels for each method.

Table 3
Summary of Detection Limits at $e = 0.0$

	Mean *K* Velocity Recovered (m s^{-1})			
Star	99% Recovery Method 1	99% Recovery Method 2	50% Recovery Method 1	50% Recovery Method 2
HD 1581	12.6 ± 1.1	4.8 ± 2.2	6.0 ± 0.5	2.8 ± 0.6
HD 4308	5.9 ± 0.1	4.7 ± 2.0	3.2 ± 0.1	2.7 ± 0.8
HD 10360	11.9 ± 0.3	9.6 ± 1.8	3.4 ± 0.1	7.0 ± 3.1
HD 10361	14.2 ± 0.3	7.9 ± 2.0	3.4 ± 0.1	5.6 ± 2.5
HD 10700	5.0 ± 0.2	3.5 ± 0.9	2.8 ± 0.1	2.4 ± 0.4
HD 16417	5.8 ± 0.3	5.9 ± 2.5	3.1 ± 0.2	3.4 ± 0.9
HD 20794	4.8 ± 0.1	4.3 ± 1.0	2.4 ± 0.1	2.7 ± 0.5
HD 23249	12.7 ± 3.0	4.6 ± 1.9	6.2 ± 1.4	2.8 ± 0.7
HD 26965	5.3 ± 0.6	8.3 ± 3.7	2.5 ± 0.3	6.2 ± 1.8
HD 28255A	34.2 ± 10.2	14.1 ± 3.2	8.8 ± 2.4	11.4 ± 5.5
HD 43834	4.6 ± 0.4	6.3 ± 2.1	2.5 ± 0.2	4.0 ± 0.8
HD 53705	5.7 ± 0.3	5.0 ± 2.6	3.1 ± 0.2	3.0 ± 0.9
HD 72673	14.5 ± 0.5	5.4 ± 2.8	3.3 ± 0.1	4.7 ± 4.3
HD 73524	14.4 ± 1.2	8.6 ± 3.8	4.1 ± 0.3	6.8 ± 4.0
HD 84117	7.9 ± 0.1	7.9 ± 3.4	4.1 ± 0.1	5.1 ± 1.5
HD 100623	6.5 ± 0.8	7.2 ± 3.5	2.9 ± 0.4	4.8 ± 1.5
HD 102365	5.6 ± 0.1	3.9 ± 1.6	2.9 ± 0.1	2.5 ± 0.6
HD 114613	8.3 ± 0.1	6.7 ± 2.9	4.3 ± 0.1	4.5 ± 1.0
HD 115617	4.0 ± 0.2	7.3 ± 3.2	2.4 ± 0.1	4.8 ± 1.4
HD 122862	8.9 ± 1.1	6.4 ± 2.0	4.0 ± 0.5	4.8 ± 1.7
HD 128620	19.4 ± 2.3	4.8 ± 2.3	3.1 ± 0.3	4.1 ± 3.6
HD 128621	16.7 ± 0.7	8.6 ± 8.1	3.1 ± 0.1	6.0 ± 4.5
HD 136352	6.0 ± 0.4	7.4 ± 2.8	3.1 ± 0.2	5.0 ± 1.4
HD 146233	6.2 ± 0.1	6.9 ± 2.6	3.2 ± 0.1	4.2 ± 1.2

3.2. Comparing the Methods

In general, the results from the two methods are in agreement, though for $P < 10$ days, Method 1 gives mass limits higher than Method 2 by a factor of 2–4 (cf. Figure 1). The reason for this difference is that Method 1 incorporates the added criterion that the semi-amplitude *K* of the recovered Keplerian orbit must satisfy $K/\sigma_K > 2$. Removing this criterion results in an extremely high proportion of false positives (incorrect detections). Method 2, with a periodogram recovery, has no such constraint on the amplitude, only on the period. Both are more conservative than a human would be in analyzing an individual observed data set by hand. On the other hand, they have a quantitative selection process which means that, given their detection criteria and a set of data, one can use these algorithms to draw robust conclusions about planetary frequency and orbital parameter distribution.

Both Methods 1 and 2 address the question of "What planets could have been detected by these data?" In any such detection-limit determination, the aim is to automate and perform thousands of times what a human investigator would reasonably do to detect a signal (O'Toole et al. 2009a). This process necessarily involves some sacrifices. For example, Method 2 attempts to detect an injected signal using the standard Lomb–Scargle periodogram, an extremely fast computation. However, the Lomb–Scargle periodogram is most efficient at detecting sinusoidal signals; when Keplerian orbits become moderately eccentric, their shapes can become significantly non-sinusoidal

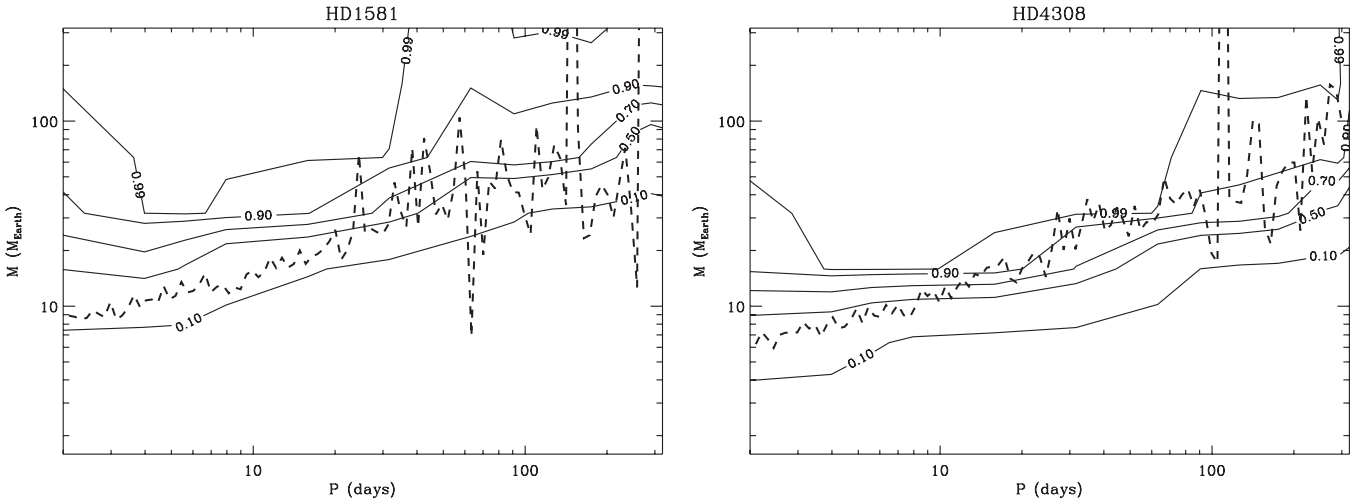

Figure 2. Detectabilities obtained from Method 1 (solid contours), for HD 1581 (left panel) and HD 4308 (right panel), for planets with eccentricities from 0.0 to 0.6. Contours indicate the fraction of injected planets that were recovered. Results from Method 2 (99% recovery) for the same range of eccentricities are overplotted as a dotted line.

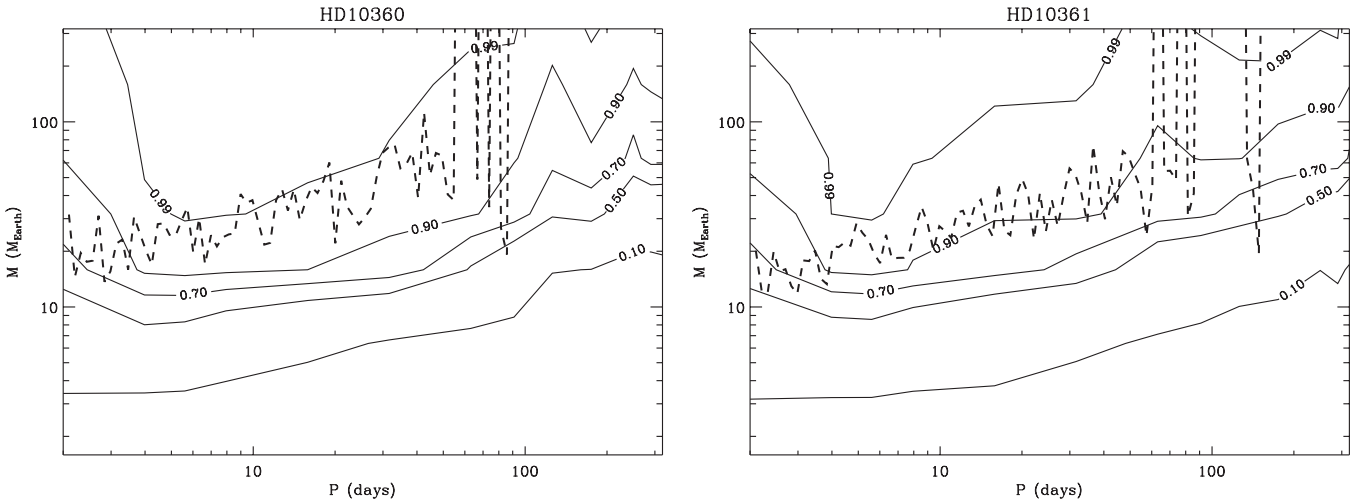

Figure 3. Same as Figure 2, but for HD 10360 (left) and HD 10361 (right).

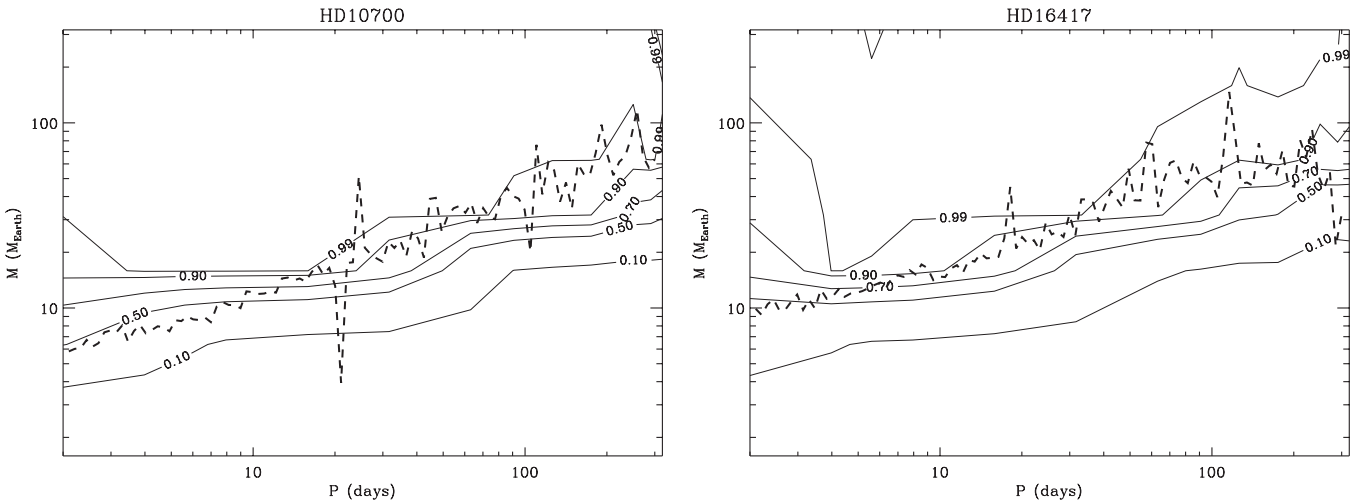

Figure 4. Same as Figure 2, but for HD 10700 (left) and HD 16417 (right).

(Cumming et al. 2008; O'Toole et al. 2009a; Wittenmyer et al. 2009). To work around this issue, Wittenmyer et al. (2006) restricted the eccentricities of the injected planets to $e < 0.6$, a range which includes about 90% of known exoplanets. The effects of eccentricity remain evident, however, in the "blind spots" where Method 2 indicates that planets at certain periods

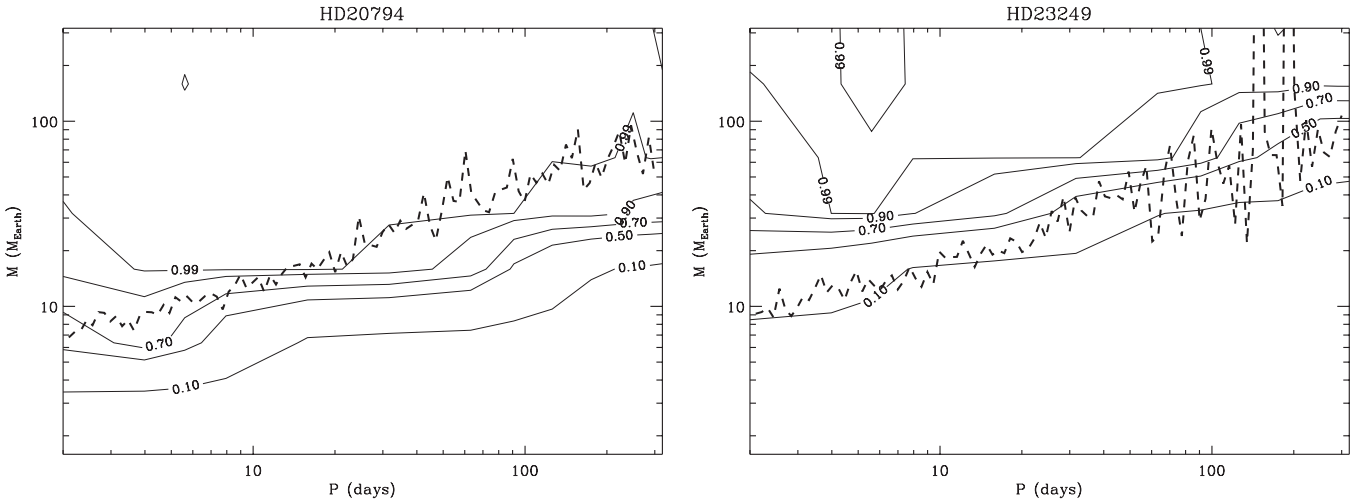

Figure 5. Same as Figure 2, but for HD 20794 (left) and HD 23249 (right).

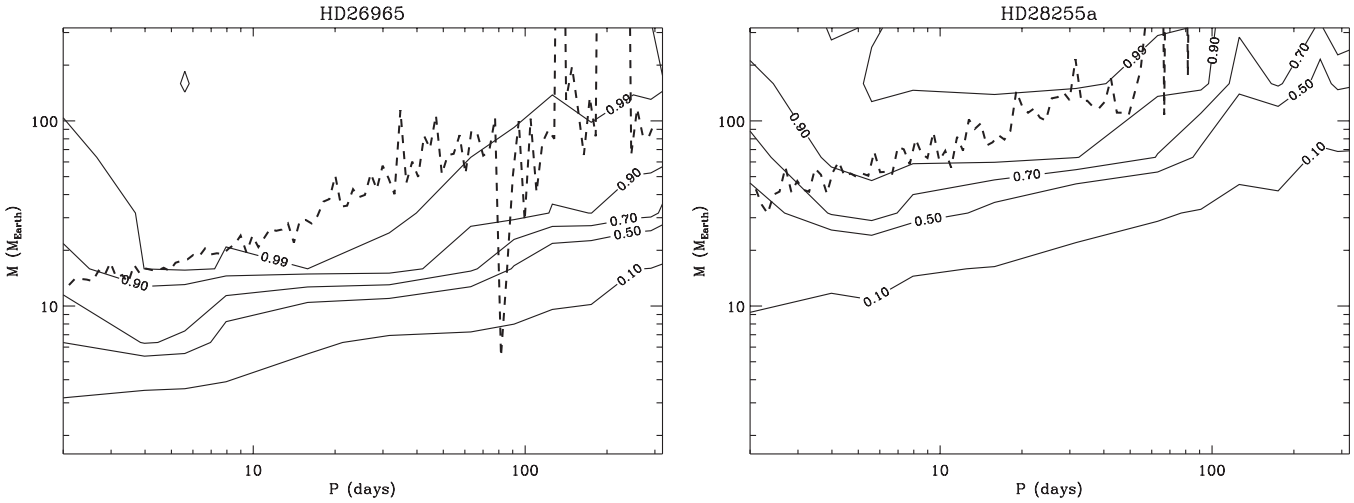

Figure 6. Same as Figure 2, but for HD 26965 (left) and HD 28255A (right).

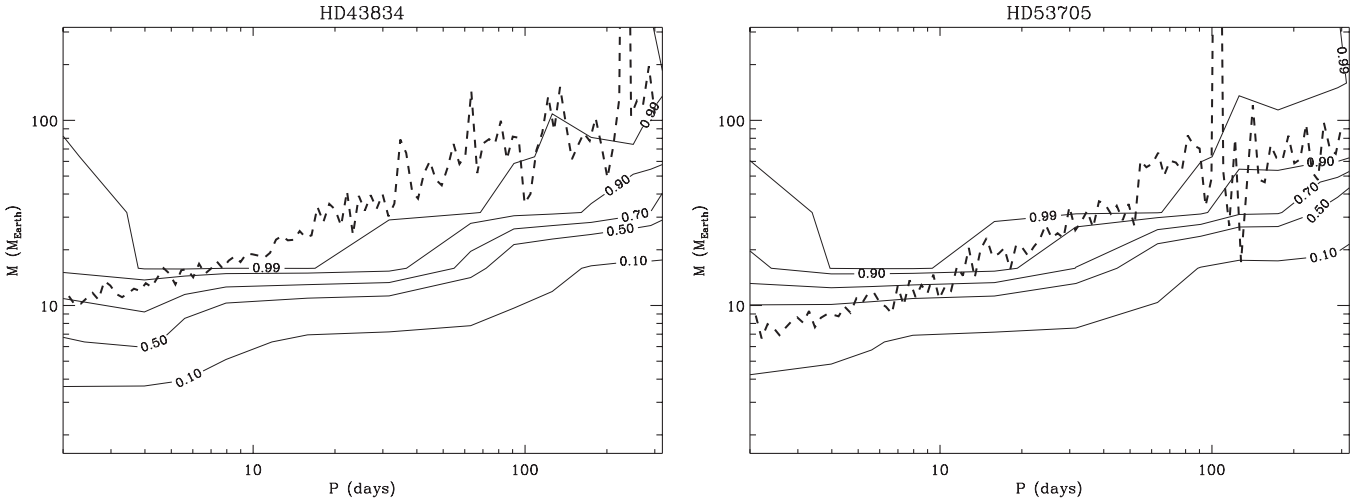

Figure 7. Same as Figure 2, but for HD 43834 (left) and HD 53705 (right).

are completely undetectable (Figure 14). For each star, there are certain trial periods where the data sampling conspires with an injected eccentric signal, such that an ordinary Lomb–Scargle periodogram does *not* exhibit a significant peak at that period. Method 2 would then reject the trial signal, even at a large amplitude ($K_{\max} = 100\,\mathrm{m\,s^{-1}}$), and these situations result in allegedly undetectable trial signals. Method 1, however, using the Two-dimensional Keplerian Lomb–Scargle (2DKLS) periodogram

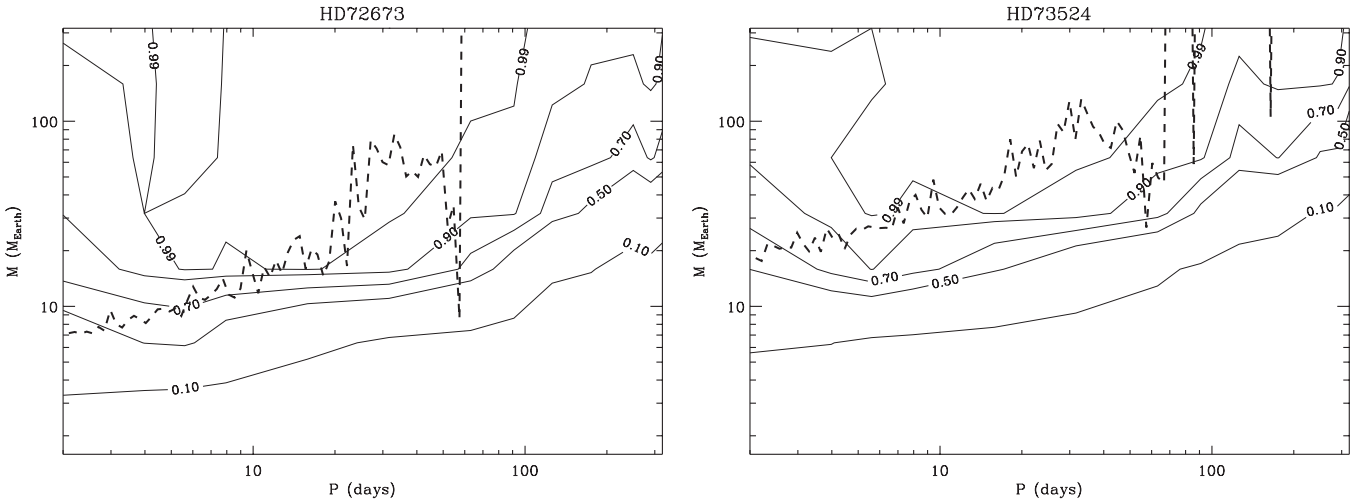

Figure 8. Same as Figure 2, but for HD 72673 (left) and HD 73524 (right).

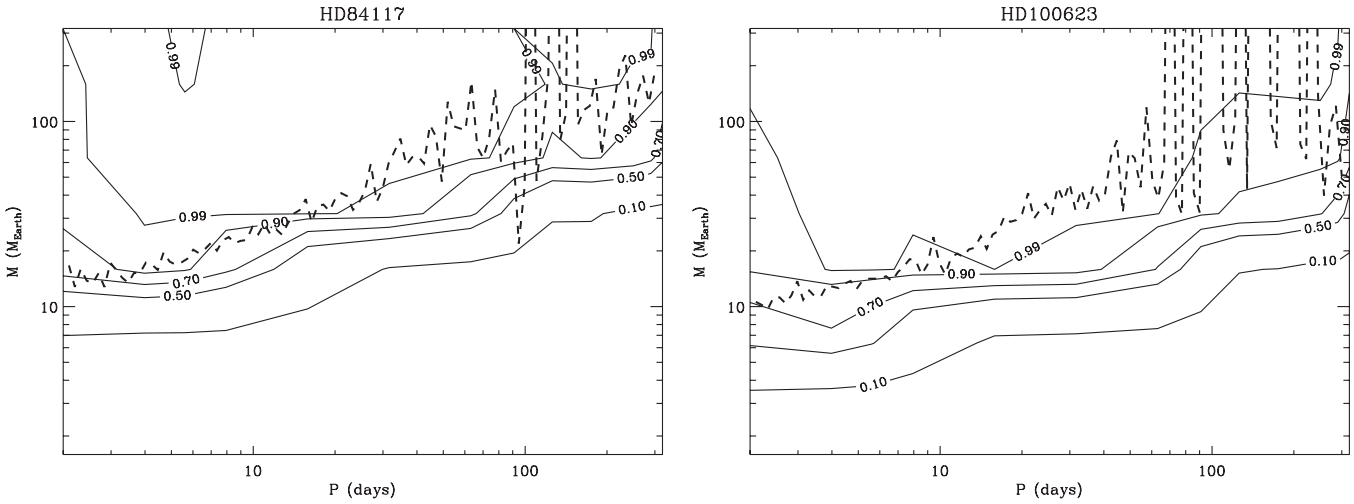

Figure 9. Same as Figure 2, but for HD 84117 (left) and HD 100623 (right).

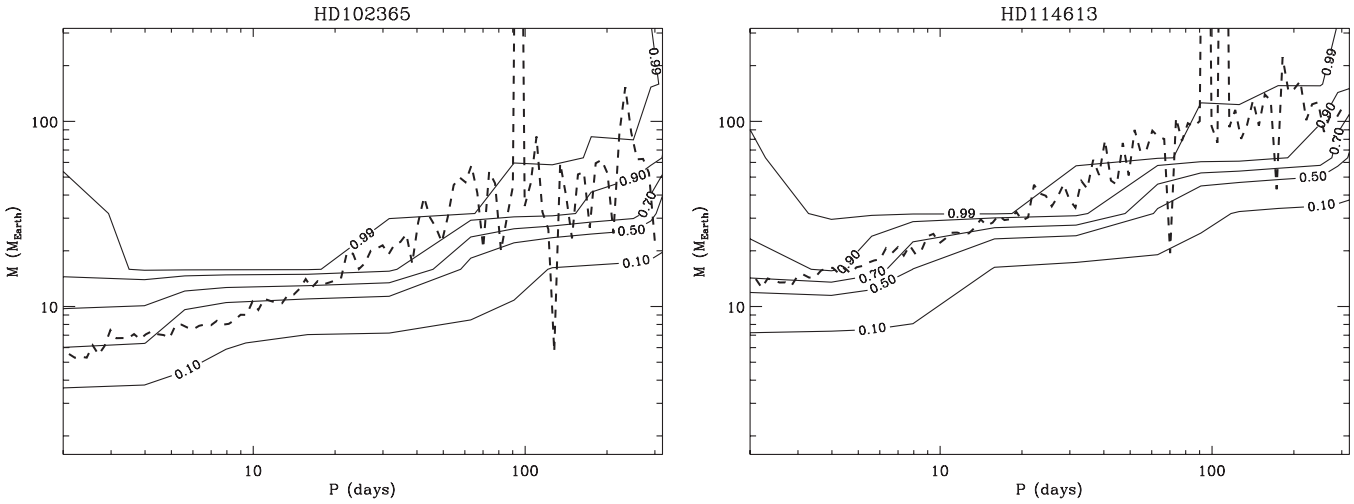

Figure 10. Same as Figure 2, but for HD 102365 (left) and HD 114613 (right).

(O'Toole et al. 2007) which is much more effective at detecting eccentric signals, would not fall victim to this pathology.

The significance of a periodogram peak obtained by Method 2 is computed using the analytic formula given in Horne & Baliunas (1986). However, the FAP obtained by this formula tends to be smaller (i.e., more significant) than that obtained by a bootstrap randomization procedure (Kürster et al. 1997). This is due to the fact that noise in radial-velocity data tends to be non-Gaussian. Thus, a human would visually inspect the periodogram, then perform a bootstrap FAP calculation to obtain an accurate estimate of the believability of any peaks. The bootstrap FAP method, however, requires hours to calculate,

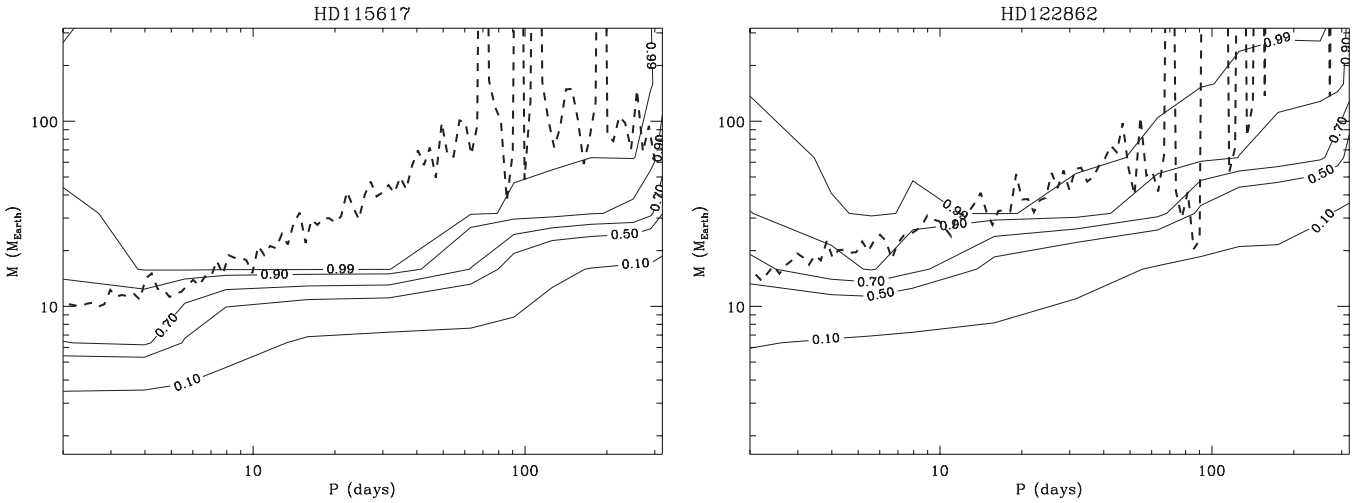

Figure 11. Same as Figure 2, but for HD 115617 (left) and HD 122862 (right).

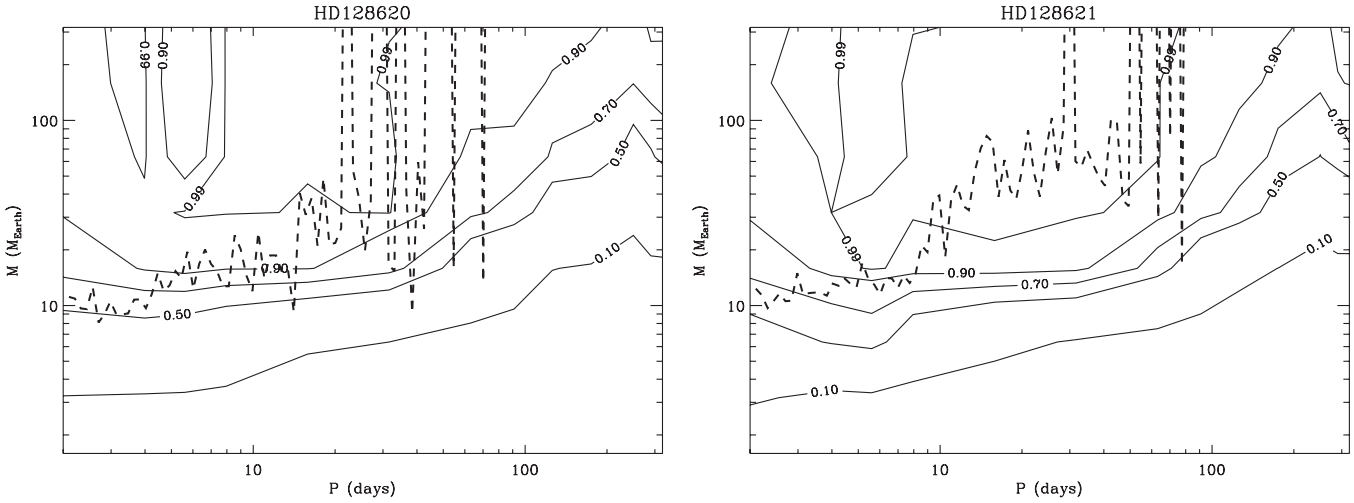

Figure 12. Same as Figure 2, but for HD 128620 (left) and HD 128621 (right).

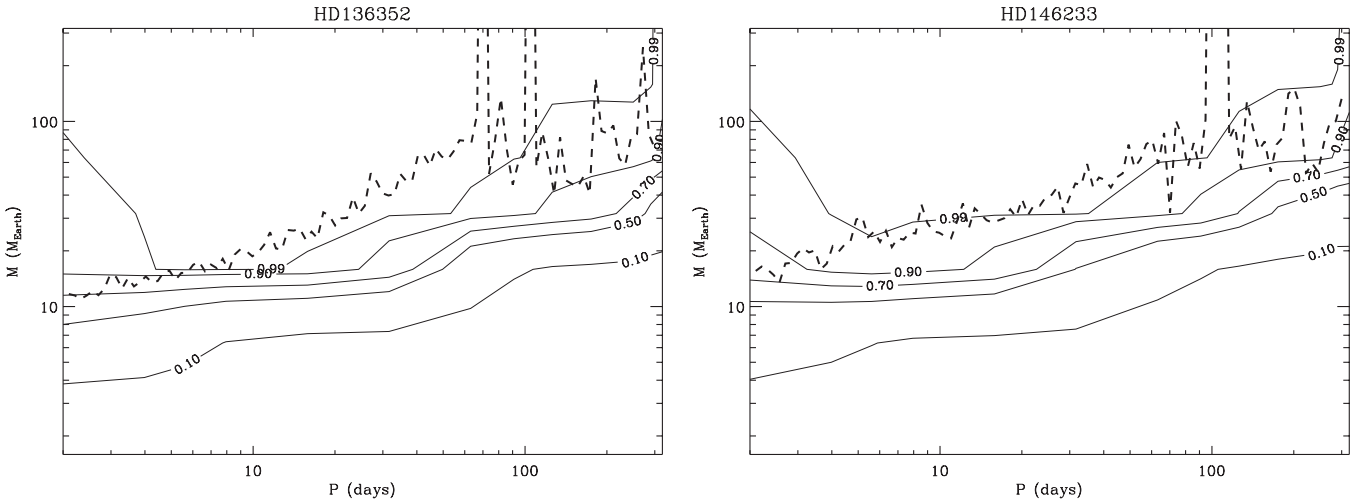

Figure 13. Same as Figure 2, but for HD 136352 (left) and HD 146233 (right).

rather than the milliseconds it takes for the analytic method, and can therefore not be usefully employed in the analysis of tens of thousands of simulations.

Another necessary concession is the requirement that the recovered period be within 5% of the injected period. The purpose of this constraint is to exclude significant periodogram peaks at aliases of the true period. Spurious periods were also often produced by the lunar cycle (∼30 days) and the duration of the densely sampled "Rocky Planet Search" (48 days). All previously published work using this method (Wittenmyer et al.

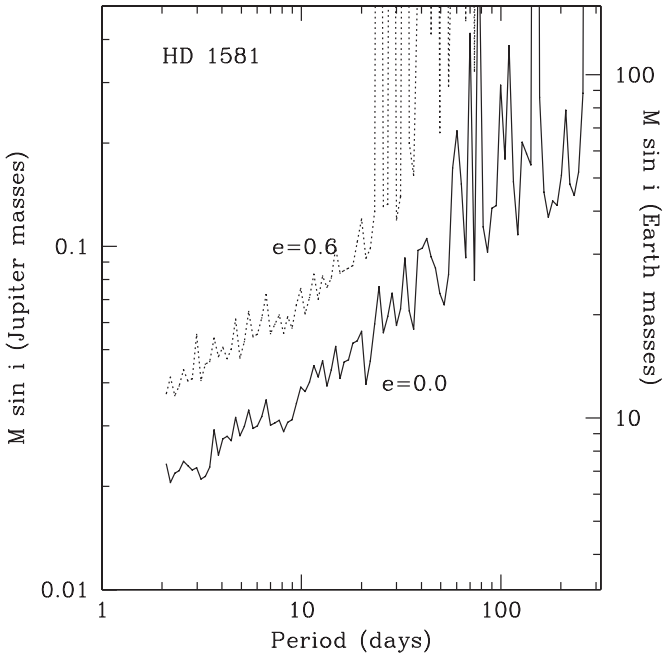

Figure 14. Detection limits for HD 1581 (Method 2) for test signals with $e = 0.0$ (solid line) and $e = 0.6$ (dashed line). At higher eccentricities, there arise some periods for which the test signal is never recovered at sufficient significance by the traditional Lomb–Scargle periodogram.

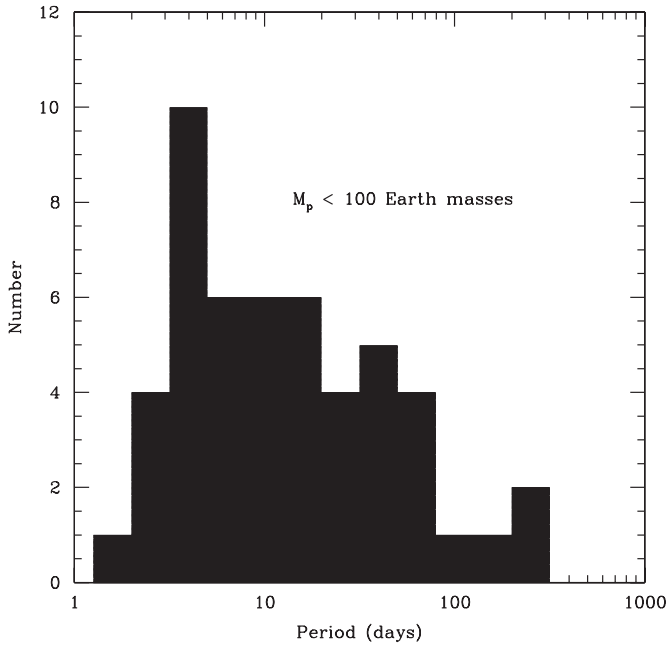

Figure 15. Observed orbital period distribution of radial-velocity planets with $m \sin i < 100\,M_\oplus$ ($N = 50$). The falloff at $P > 5$ days arises from the twin selection effects of smaller velocity amplitudes and poorer temporal sampling, especially in the period range of 30–50 days.

2006, 2007, 2009) has used this 5% criterion. This has the effect of preventing incorrect detections (false positives). Method 1 does not have an explicit criterion of this sort, but the four criteria outlined in Section 2.1 serve to keep the rate of false positives below ∼1%–2%; a detailed discussion of false positives is given in O'Toole et al. (2009a).

To summarize, Method 1 seems to be most appropriate for significantly eccentric orbits because the simulated planets are fitted with a full Keplerian model. Since a value of stellar velocity noise (jitter) is added to the simulated data in Method 1 that method is more effective when the radial-velocity noise is well understood. If the stellar jitter is not well understood, it is more appropriate to use Method 2 since the actual velocity data (which include all noise sources) are used.

4. DISCUSSION

4.1. $M_p > 100\,M_\oplus$

Jones et al. (2003) and Udry et al. (2003) noted an emerging "period valley" between 10 and 100 days; the ∼250 additional planets discovered since then have continued this trend. Udry et al. (2003) also showed that this feature is mainly attributable to the lack of massive ($m \sin i > 2\,M_{\rm Jup}$) planets in that period range. Our results support this claim, since the 24-star sample contains three low-mass planets with periods between 10 and 100 days (HD 4308b, HD 16417b, and HD 115617c), and the data can exclude planets with $m \sin i > 0.5\,M_{\rm Jup}$ at the 99% level for all of this region (Figure 1). The deficit of higher-mass planets with $P < 300$ days is readily apparent, suggesting that the period valley is not a selection effect; this is consistent with the conclusions reached by Cumming et al. (2008).

4.2. $M_p < 100\,M_\oplus$

At lower masses (10–100 $M_\oplus$), however, the situation is far less clear. This is an extremely interesting mass range, as core-accretion theory, and numerical simulations based on it predict a "planet desert" to arise from rapid gas accretion by cores once they reach about 10 $M_\oplus$ (Ida & Lin 2004, 2008a; Liu et al. 2009). Recent simulations by Liu et al. (2009) showed a pile-up of planets at 0.2–0.3 AU ($P \sim 30$–50 days). This is a mass range, then, which *should* show detectable features in the structure of the period distribution. However, this is also a mass range at which serious selection effects impact on the detectability of low-mass planets and most especially in the critical 15–60 day orbital period range. This is why Liu et al. (2009) noted that the predicted pile-up had not yet been observed. Figure 15 shows the period distribution of planets with $M_p < 100\,M_\oplus$. A steep falloff in the distribution is evident at $P \gtrsim 5$ days. This can be understood as arising from two selection effects. First and most obviously, longer-period planets have weaker radial-velocity signals. Second, planet search observing runs are almost exclusively scheduled on large telescopes during bright time, resulting in large peaks in the window function at 28 days. The only means to mitigate this sampling problem is to observe through dark lunations. This is a strategy that only the AAPS is currently employing in its "Rocky Planet Search" observing campaigns and which (as demonstrated by the discovery of 61 Vir c, $P = 38$ days, $K = 3.6$ m s^{-1}) has proven successful in finding low-mass planets in this period range.

When observing strategies are employed which mitigate selection effects in this period regime, we do indeed find low-mass planets (e.g., Vogt et al. 2010; O'Toole et al. 2009b). These discoveries indicate that the observed falloff in the distribution of such planets (Figure 15) may—contrary to what is seen at higher masses—indeed merely be a result of observational biases. If we look at the results of our simulations, they indicate that 10% of planets with $K \sim 2.7$ m s^{-1} could have been detected in our sample of 24 stars. One such planet with an even smaller radial-velocity amplitude has actually been discovered in our sample (61 Vir b, $K = 2.2$ m s^{-1}), suggesting that at least a further nine more such planets could have been missed and will

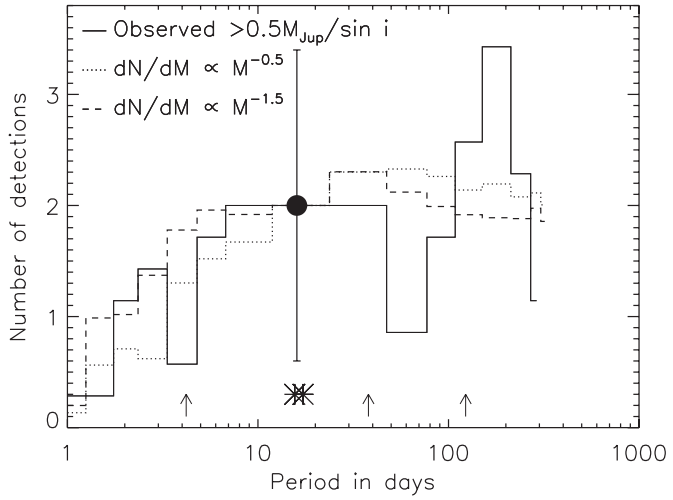

Figure 16. Solid-line histogram: orbital period distribution of radial-velocity exoplanets with $m \sin i > 0.5\ M_{\rm Jup}$ ($N = 256$); both simulation methods discussed in this work show that all of the planets this massive would have been detected in our sample, indicating that the lack of giant planets with $P < 100$ days does not arise from selection biases. Overplotted as dashed and dotted histograms are orbital period distributions that would be expected from our simulations, for a variety of assumed power-law mass functions. Asterisks show the periods of announced exoplanets from our sample that are redetected by our automated selection criteria (Section 2), while arrows show the periods of the three planets detected orbiting 61 Vir (using a combination of AAPS and Keck data), which are *not* redetected by our automated criteria with AAPS data alone.

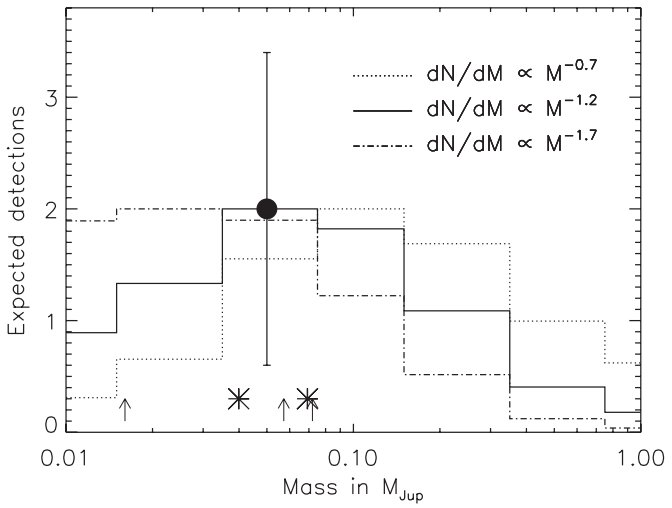

Figure 17. Expected number of exoplanets from our sample as a function of mass, for different mass functions including logarithmic migration. Asterisks and arrows show the mass of announced exoplanets from our sample, as for Figure 16. The heavy filled circle with uncertainties shows the number density represented by our automated system detections in the $0.05 M_{\rm Jup}$ bin, while arrows show the periods of the three planets detected orbiting 61 Vir (using a combination of AAPS and Keck data), which are *not* redetected by our automated criteria with AAPS data alone.

remain below the detection threshold until additional data are obtained.

In addition, the solar-type dwarf stars typically observed by precision radial-velocity programs have typical rotation periods in the 20–50 day range. Hence, emergent periodicities are not usually believed until sufficient data are in hand to be confident that the periodicity is planetary in origin rather than due to rotational modulation by starspots. This selection bias suggests that low-mass planets with $P \sim 30$–50 days may be present in extant radial-velocity data sets, but as yet not believed and unpublished.

4.3. The Underlying Planetary Mass Function

The importance of planetary migration has been appreciated for some time (Goldreich & Tremaine 1980; Lin & Papaloizou 1986). The modeling work of Trilling et al. (2002) and Armitage et al. (2002) has provided evidence that observational data for exoplanets are consistent with a model where planets are formed at around 5 AU and then undergo migration. This leads to a distribution of planetary semimajor axis a that depends on $\log(a)$. Although this scenario provides a good match to observations (e.g., Armitage 2007), migration rates at short orbital periods are expected to be different for different mass planets. The simulations of Rice et al. (2008) indicate three regimes: (1) low-mass planets ($<0.5\ M_{\rm Jup}$) migrate inward and stall at approximately half the rotation period of the star, (2) high-mass planets ($10\ M_{\rm Jup}$) should collide with the star, and (3) the intermediate-mass ($1\ M_{\rm Jup}$) planets population should have an inner edge located at twice the Roche limit (Rasio & Ford 1996). For the purposes of our models, we implement a distribution of planetary semimajor axis that depends on $\log(a)$, referred to here as "logarithmic migration."

Although our target star sample and the number of detections are small, we can use the fact that it is well characterized in an attempt to understand the features of the larger inhomogeneous data set of radial-velocity exoplanets. Following the work of O'Toole et al. (2009c) and using our computed detectabilities and a simplistic logarithmic migration (Armitage 2007), Figure 16 shows the expected number of planets for different underlying mass functions as a function of the semimajor axis for the case of equal numbers of exoplanets in each bin. The bold asterisks represent the planets detected from this sample (Table 2). We find that the total expected number of detections for different assumed mass functions observed with our sample varies by a factor of about two for the mass functions shown, with all giving a smooth falloff in the number of detections toward longer periods. Thus, although the peak of the histogram serves to approximately characterize our detection of two exoplanets in the 10–20 day period bin and is consistent with those below the threshold, the clear rise at longer periods in the observed distribution in Figure 16 is not reproduced. However, it must be noted that the sample of all radial-velocity exoplanets shown in Figure 16 is highly inhomogeneous and represents an observed sample of a higher mass range.

Although Figure 16 indicates that the distribution in period space is relatively insensitive to different mass functions, we find greater sensitivity when detectability is plotted as a function of mass. Following O'Toole et al. (2009c), we show in Figure 17 the expected detections for our sample as a function of mass for a variety of assumed mass functions. We find that the peak in the expected number of *observed* exoplanets moves for different mass functions. $\alpha = -1.7$ leads to a peak in the number of detected planets around $0.02\ M_{\rm Jup}$ ($6.3\ M_{\oplus}$), the $\alpha = -1.2$ expected detections peak at around $0.05\ M_{\rm Jup}$ ($16\ M_{\oplus}$) while the flatter $\alpha = -0.7$ mass function produces an expected detection peak at around $0.10\ M_{\rm Jup}$ ($32\ M_{\oplus}$).

Given that we have found two exoplanet signals in the 16–25 $M_{\oplus}$ minimum mass range (corresponding to the $0.05\ M_{\rm Jup}$ or $16\ M_{\oplus}$ bin in Figure 17), we may consider these as providing rough limits on the underlying mass function as determined by how changes in the mass function cause the peak of detections to

move toward and away from the 0.05 $M_{\rm Jup}$ (16 $M_{\oplus}$) bin. We find that the peak moves from the 0.02 to the 0.05 $M_{\rm Jup}$ bin for α values shallower than $\alpha = -1.6$ and from 0.05 $M_{\rm Jup}$ to 0.1 $M_{\rm Jup}$ at $\alpha = -1.1$. It is noteworthy that the peak mass for different mass functions is sensitive to migration. If no migration is employed then the mass function peak moves away from the 0.05 $M_{\rm Jup}$ (16 $M_{\oplus}$) bin when $0.6 \leqslant \alpha \leqslant 1.2$. Based on Poisson-counting statistics of two detections our simulations indicate a normalization of 0.17 $\pm$ 0.12 (corresponding to the F value presented in O'Toole et al. 2009c). Our estimate of the underlying mass function shown in Figure 17 is consistent with the first attempt presented in O'Toole et al. (2009c). That is, the additional planet detections in this sample and the comprehensive detection limits presented here serve to strengthen the case for an underlying planet mass function of the form $dN/dM \propto M^{-1.0}$. Given that we robustly do not detect more massive planets in this sample, flatter mass functions are not favored.

5. CONCLUSIONS

We have shown, using two independent simulation algorithms, that recent data from the AAPS are capable of placing meaningful limits on the population of potentially terrestrial, sub-Neptune-mass planets orbiting nearby stars. As we are able to detect all planets with at least a Saturn mass in the period range $P < 300$ days, we conclude that the observed lack of massive planets ($M_p > 100\,M_{\oplus}$) with periods 10–100 days is real and not due to selection effects. However, we conclude that the shortage of lower-mass planets ($M_p < 100\,M_{\oplus}$) predicted by core-accretion theory in this period range may arise from observational selection biases against detecting such planets.

We gratefully acknowledge the UK and Australian government support of the Anglo-Australian Telescope through their PPARC, STFC, and DIISR funding; STFC grant PP/C000552/1, ARC Grant DP0774000, and travel support from the Anglo-Australian Observatory. R.W. is supported by a UNSW Vice-Chancellor's Fellowship.

Exoplanet data were obtained from the Extrasolar Planets Encyclopedia (http://exoplanet.eu/) maintained by Jean Schneider. This research has made use of NASA's Astrophysics Data System (ADS), and the SIMBAD database, operated at CDS, Strasbourg, France.

REFERENCES

Adams, E. R., Seager, S., & Elkins-Tanton, L. 2008, ApJ, 673, 1160
Armitage, P. J. 2007, ApJ, 665, 1381
Armitage, P. J., Livio, M., Lubow, S. H., & Pringle, J. E. 2002, MNRAS, 334, 248
Bonfils, X., et al. 2005, A&A, 443, L15
Cumming, A., Butler, R. P., Marcy, G. W., Vogt, S. S., Wright, J. T., & Fischer, D. A. 2008, PASP, 120, 531
Cumming, A., Marcy, G. W., & Butler, R. P. 1999, ApJ, 526, 890
Endl, M., Kürster, M., Els, S. H. A. P., Cochran, W. D., Dennerl, K., & Döbereiner, S. 2002, A&A, 392, 671
Goldreich, P., & Tremaine, S. 1980, ApJ, 241, 425
Horne, J. H., & Baliunas, S. L. 1986, ApJ, 302, 757
Ida, S., & Lin, D. N. C. 2004, ApJ, 604, 388
Ida, S., & Lin, D. N. C. 2008a, ApJ, 673, 487
Ida, S., & Lin, D. N. C. 2008b, ApJ, 685, 584
Jones, H. R. A., Butler, R. P., Tinney, C. G., Marcy, G. W., Penny, A. J., McCarthy, C., & Carter, B. D. 2003, MNRAS, 341, 948
Kürster, M., Schmitt, J. H. M. M., Cutispoto, G., & Dennerl, K. 1997, A&A, 320, 831
Lin, D. N. C., & Papaloizou, J. 1986, ApJ, 309, 846
Liu, H., Zhou, J.-l., & Wang, S. 2009, arXiv:0912.1770
Lomb, N. R. 1976, Ap&SS, 39, 447
Mayor, M., & Queloz, D. 1995, Nature, 378, 355
McArthur, B. E., et al. 2004, ApJ, 614, L81
O'Toole, S. J., Tinney, C. G., & Jones, H. R. A. 2008, MNRAS, 386, 516
O'Toole, S. J., Tinney, C. G., Jones, H. R. A., Butler, R. P., Marcy, G. W., Carter, B., & Bailey, J. 2009a, MNRAS, 392, 641
O'Toole, S. J., et al. 2007, ApJ, 660, 1636
O'Toole, S., et al. 2009b, ApJ, 697, 1263
O'Toole, S., et al. 2009c, ApJ, 701, 1732
Rasio, F. A., & Ford, E. B. 1996, Science, 274, 954
Rice, W. K. M., Armitage, P. J., & Hogg, D. F. 2008, MNRAS, 384, 1242
Santos, N. C., et al. 2004, A&A, 426, L19
Scargle, J. D. 1982, ApJ, 263, 835
Seager, S., Kuchner, M., Hier-Majumder, C. A., & Militzer, B. 2007, ApJ, 669, 1279
Sudarsky, D., Burrows, A., & Pinto, P. 2000, ApJ, 538, 885
Trilling, D. E., Lunine, J. I., & Benz, W. 2002, A&A, 394, 241
Udry, S., Mayor, M., & Santos, N. C. 2003, A&A, 407, 369
Udry, S., et al. 2006, A&A, 447, 361
Vogt, S. S., et al. 2010, ApJ, 708, 1366
Walker, G. A. H., Walker, A. R., Irwin, A. W., Larson, A. M., Yang, S. L. S., & Richardson, D. C. 1995, Icarus, 116, 359
Wittenmyer, R. A., Endl, M., Cochran, W. D., Hatzes, A. P., Walker, G. A. H., Yang, S. L. S., & Paulson, D. B. 2006, AJ, 132, 177
Wittenmyer, R. A., Endl, M., Cochran, W. D., & Levison, H. F. 2007, AJ, 134, 1276
Wittenmyer, R. A., Endl, M., Cochran, W. D., Levison, H. F., & Henry, G. W. 2009, ApJS, 182, 97